Hyperfine Interact
DOI 10.1007/s10751-015-1202-4

Antiproton cloud compression in the ALPHA apparatus at CERN

A. Gutierrez[1] · M. D. Ashkezari[2] · M. Baquero-Ruiz[3] · W. Bertsche[4,5] · C. Burrows[6] · E. Butler[7,8] · A. Capra[9] · C. L. Cesar[10] · M. Charlton[6] · R. Dunlop[2] · S. Eriksson[6] · N. Evetts[1] · J. Fajans[3] · T. Friesen[11] · M. C. Fujiwara[12] · D. R. Gill[12] · J. S. Hangst[11] · W. N. Hardy[1] · M. E. Hayden[2] · C. A. Isaac[6] · S. Jonsell[13] · L. Kurchaninov[12] · A. Little[3] · N. Madsen[6] · J. T. K. McKenna[12] · S. Menary[9] · S. C. Napoli[13] · P. Nolan[14] · K. Olchanski[12] · A. Olin[12] · P. Pusa[14] · C. Ø. Rasmussen[11] · F. Robicheaux[15] · R. L. Sacramento[10] · E. Sarid[16] · D. M. Silveira[10] · C. So[3] · S. Stracka[12] · J. Tarlton[7] · T. D. Tharp[11] · R. I. Thompson[17] · P. Tooley[4] · M. Turner[3] · D. P. van der Werf[6] · J. S. Wurtele[3] · A. I. Zhmoginov[3]

Abstract We have observed a new mechanism for compression of a non-neutral plasma, where antiprotons embedded in an electron plasma are compressed by a rotating wall drive at a frequency close to the sum of the axial bounce and rotation frequencies. The radius of the antiproton cloud is reduced by up to a factor of 20 and the smallest radius measured is ~ 0.2 mm. When the rotating wall drive is applied to either a pure electron or pure antiproton plasma, no compression is observed in the frequency range of interest. The frequency range over which compression is evident is compared to the sum of the antiproton bounce

Proceedings of the 6th International Conference on Trapped Charged Particles and Fundamental Physics (TCP 2014), Takamatsu, Japan, 1–5 December 2014

✉ A. Gutierrez
andrea.gutierrez@triumf.ca

[1] Department of Physics and Astronomy, University of British Columbia, Vancouver, British Columbia V6T 1Z1, Canada

[2] Department of Physics, Simon Fraser University, Burnaby, British Columbia, V5A 1S6, Canada

[3] Department of Physics, University of California at Berkeley, Berkeley, CA 94720-7300, USA

[4] School of Physics and Astronomy, University of Manchester, M13 9PL Manchester, UK

[5] The Cockcroft Institute, WA4 4AD Warrington, UK

[6] Department of Physics, College of Science, Swansea University, Swansea SA2 8PP, UK

[7] Centre for Cold Matter, Imperial College, London SW7 2BW, UK

Published online: 12 October 2015

frequency and the system's rotation frequency. It is suggested that bounce resonant transport is a likely explanation for the compression of antiproton clouds in this regime.

Keywords Antiprotons · Rotating wall · Compression · Electrons · Penning-Malmberg trap · Non-neutral plasma · Antihydrogen

1 Introduction

Antihydrogen is the simplest neutral antimatter atom. Precision comparisons between hydrogen and antihydrogen would provide stringent tests of the CPT (charge conjugation/parity transformation/time reversal) invariance and the weak equivalence principle [1]. In the last few years, the ALPHA collaboration has produced [2], and trapped antihydrogen [3, 4]. Recently, ALPHA studied antihydrogen's internal structure by inducing hyperfine transitions in ground state atoms [5].

In order to form antihydrogen, antiprotons and positrons are first stored in the form of non-neutral plasmas in Penning-Malmberg traps [6] and then, are allowed to interact to form antihydrogen [7].

The radial compression of antiproton, electron and positron plasmas is necessary to counteract expansion drag due to asymmetries in the static fields and the presence of background gases [8–10], and thereby attain long confinement times. Moreover, radial compression allows control of the radial sizes and densities of the non-neutral plasmas [11]. A commonly-used technique is the rotating wall (RW), in which a time-varying azimuthal rotating electric field is used to balance or exceed the drag by applying a positive torque to the plasma (see e.g., [6, 12]).

Antiproton cloud compression is an important tool for the formation and trapping of cold antihydrogen. Decreasing the antiproton cloud's radius reduces the circumferential velocity of the antiprotons and results in antihydrogen atoms with lower kinetic energy [13]. Additionally, ALPHA's magnetic trap is used to confine low energy antihydrogen atoms and it is composed of an octupole magnet providing a transverse magnetic field, plus two mirror coils [14]. The transverse magnetic field breaks the cylindrical symmetry of the

[8] Physics Department, CERN, CH-1211 Geneva 23, Switzerland

[9] Department of Physics and Astronomy, York University, Toronto, Ontario, M3J 1P3, Canada

[10] Instituto de Física, Universidade Federal do Rio de Janeiro, Rio de Janeiro 21941-972, Brazil

[11] Department of Physics and Astronomy, Aarhus University, DK-8000 Aarhus C, Denmark

[12] TRIUMF, 4004 Wesbrook Mall, Vancouver, British Columbia V6T 2A3, Canada

[13] Department of Physics, Stockholm University, SE-10691 Stockholm, Sweden

[14] Department of Physics, University of Liverpool, Liverpool L69 7ZE, UK

[15] Department of Physics, Purdue University, West Lafayette, Indiana 47907, USA

[16] Department of Physics, NRCN-Nuclear Research Center Negev, Beer Sheva, IL-84190, Israel

[17] Department of Physics and Astronomy, University of Calgary, Calgary, Alberta T2N 1N4, Canada

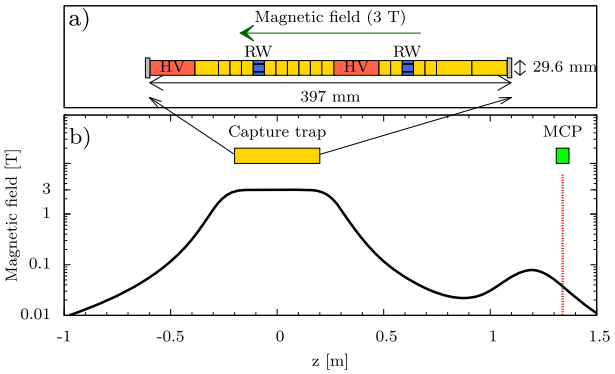

Fig. 1 a) Schematic of the electrodes making up the Penning-Malmberg trap of the antiproton capture trap. b) The magnetic field on the axis of the trap as a function of the longitudinal position. The position of the electrodes and the MCP/phosphor/CCD detector are illustrated. A small solenoid is placed at $z = 1.2$ m to guide the particles

Penning-Malmberg trap and induces non-neutral plasma diffusion [15] and ballistic loss [16]. The exposure of the plasmas to the octupole's transverse magnetic field can be minimized by reducing their radial size. Finally, the antiproton and positron plasmas should be well-overlapped to maximize the yield of antihydrogen atoms. Since radially small, dense positron plasmas are needed to increase the rate of antihydrogen production, thus radially small antiproton clouds are optimal.

Until present, two different kinds of antiproton cloud compression have been reported. In Ref. [17], in the ALPHA experiment, an electron plasma co-located in the trap was compressed by a RW in the 10 MHz region, cooling and sympathetically compressing the antiproton cloud. In this work, we present evidence of compression of antiproton clouds at low frequencies (hundreds of kHz), in a markedly different regime. Furthermore, this work is differentiated from the observations reported by the ASACUSA collaboration in Ref. [18], since we use an electron plasma as a source of cooling for the antiprotons. The presence of the electron plasma, particularly its self-electric field, greatly affects the behaviour of the system.

2 Experimental procedure

2.1 Apparatus

The upgraded ALPHA antiproton capture trap used for these experiments is a Penning-Malmberg trap with a stack of twenty cylindrical electrodes for axial confinement of charged particles, plus a 3 T solenoidal magnetic field, directed along the trap axis, to confine the charged particles radially. Figure 1a illustrates the electrode stack. Two high-voltage (HV) electrodes are used to catch and trap antiprotons from the Antiproton Decelerator [14].

The particles can be released from the trap onto a MCP/phosphor/CCD[1] detector assembly to destructively image the radial density profile [19]. The detector is shown on the right hand side of Fig. 1b, along with a plot of the axial magnetic field used to guide the particles.

[1] MCP: micro-channel plate and CCD: charge-coupled device.

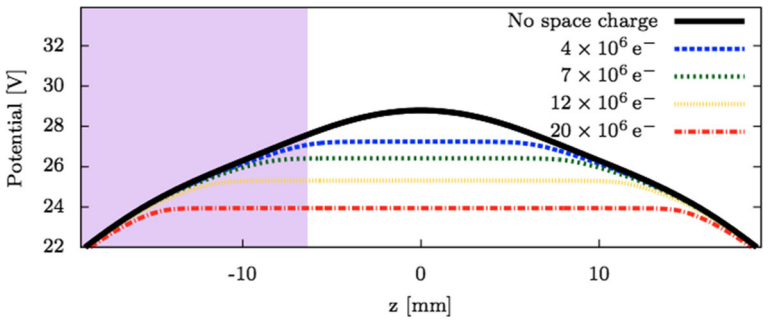

Fig. 2 Black continuous line: the electric potential well used to hold the electrons during the application of the RW. The (purple) shaded region indicates the position of the rotating wall electrode. The various dotted and dashed lines show the self-consistent potential for the numbers of electrons indicated in the legend

2.2 Antiproton capture and cooling using secondary electrons

Antiprotons are extracted from the Antiproton Decelerator into the experiment with a kinetic energy of 5.3 MeV. The energy of the antiprotons is degraded by thin layers of aluminium and beryllium, and antiprotons with an energy less than 5 keV are captured by the high-voltage electrodes [14]. The antiprotons are cooled by allowing them to interact with an electron plasma [20]. Energy is transferred to the electrons through Coulomb collisions, while the electrons cool with a time constant of about 0.4 s in the 3 T magnetic field through emission of cyclotron radiation.

Typically, the electrons are preloaded from a source, but in this work, we made use of the secondary electrons that are created when the antiprotons pass through the degrader layers. Using secondary electrons, ~ 90 % of the antiprotons are cooled while usually only ~ 60 % are cooled with preloaded electrons [17]. This increase in the cooling efficiency is due to improved radial overlap of the antiproton cloud and the secondary electrons. For every measurement, this cooling procedure results in $\sim 1.5 \times 10^5$ antiprotons and $\sim 20 \times 10^6$ electrons. If desired, a fraction of the electrons can be removed by suddenly opening one side of the trap well. Depending on the pulse time and voltage, a fraction of the electrons escape from the trap, while heavier antiprotons remain trapped [14].

2.3 Rotating wall application

The RW field is produced by an electrode divided into azimuthally isolated segments and by applying to each segment a sinusoidal potential $V_j(t)$ of frequency ω, amplitude A and phase $\theta_j = 2\pi j/k$, where k is the number of segments. The potential can be expressed as:

$$V_j(t) = A\cos(\theta_j - \omega t). \tag{1}$$

For the measurements presented in this paper, we used one of two six-segment electrodes (identified as RW in Fig. 1). For each measurement, antiprotons and electrons were captured and cooled. Then, the electron number was adjusted if necessary and the RW was applied at a fixed amplitude of 1 V for 100 s. For technical reasons, the frequency of the drive was swept over a 0.2 kHz range centred on a given frequency. After the RW application, the particles were extracted onto the MCP.

The continuous line in Fig. 2 shows the potential well used to hold the particles while the RW was applied. The potential well is almost harmonic with an antiproton bounce frequency

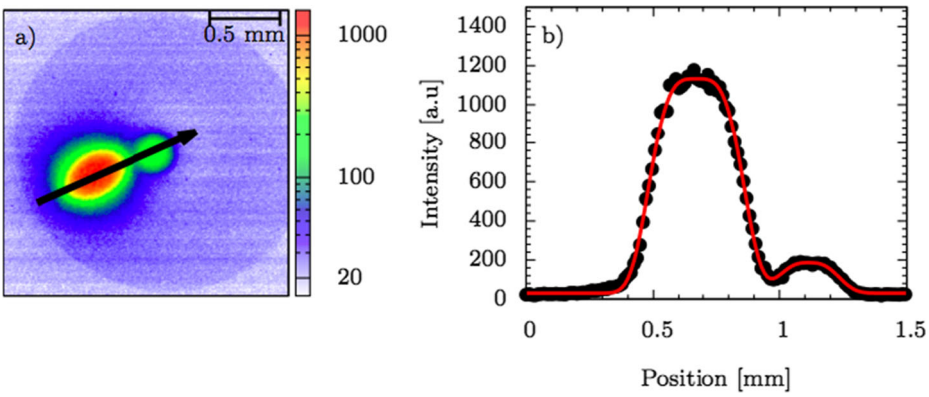

Fig. 3 a) MCP image of an antiproton-electron plasma after compression. The (black) arrow indicates the position of the profile shown in b). b) Dots are the data from the radial profile across the arrow shown in a) and the (red) curve is the respective fit

of ~ 270 kHz. When electrons are added, the shape of the potential is distorted due to their space charge. The dotted and dashed lines in Fig. 2 shows the total self-consistent potential when using 4×10^6, 7×10^6, 12×10^6 and 20×10^6 electrons, as calculated by solving Poisson's equation with a density distribution given by a Boltzmann distribution, using the self-consistent potential [6].

2.4 Analysis of MCP images

An example image of an antiproton-electron plasma is shown in Fig. 3a. Due to their mass difference, the antiprotons and electrons image to different positions on the MCP, with the antiprotons appearing on the left [19, 21]. The electron density can be conveniently described by a two-dimensional generalized Gaussian of the form $n_e \exp(|\frac{\mathbf{r}-\mathbf{r}_e}{\sigma_e}|^{k_e})$, where n_e, σ_e, $\mathbf{r}_e$ and k_e are fit parameters. For the antiproton density, we use a similar equation but modified to account for the observed elliptical shape [21]. A simultaneous fit of the two distributions is performed for each image. A cut through the image in Fig. 3a is plotted in Fig. 3b, along with the respective fit. n_e and $n_{\overline{p}}$, the central densities of the electrons and the antiprotons, respectively, are used as quantitative measures of the degree of compression.

3 Results

An image of the antiproton-electron plasma after capture and cooling is shown in Fig. 4a. We estimate that the plasma has a radius of ~ 4 mm and a rotation frequency of ~ 10 kHz. Figure 4b shows the plasma after the electron number has been reduced to 4×10^6 electrons and a RW field at a frequency of 140 kHz has been applied for 100 s. We observe that the antiproton cloud has been compressed to a radius of ~ 0.3 mm, while only a few of the electrons have been compressed. Figure 4c shows the plasma with 20×10^6 electrons after compression at 600 kHz. Similarly to the previous case, we see a dense antiproton cloud, with a radius of ~ 0.2 mm. Additionally, about 15 % of the electron plasma has also been compressed. In any of these experiments, we do not observe that the rotating wall induces any loss of antiprotons.

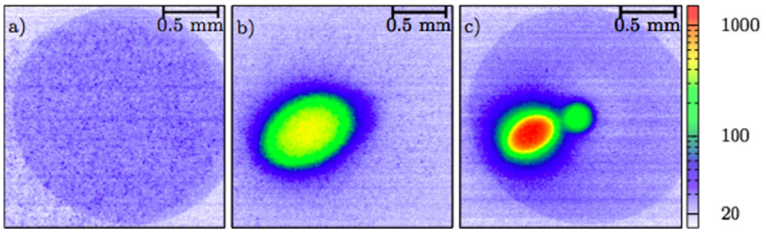

Fig. 4 a) MCP image of the antiproton-electron plasma before applying the RW. b) MCP image of the antiproton cloud co-located with 4×10^6 electrons after applying the RW at 140 kHz. c) MCP image of the antiproton cloud co-located with 20×10^6 electrons after applying the RW at 600 kHz. The clouds in image a) are too disperse to image as b) and c). The circle near the edges of images a) and c) is a mechanical aperture. The mechanical aperture is not observed in b) because the electrons are not dense enough

The striking difference that emerges when compared to the case of sympathetic compression [17] is that when the RW field is applied to a pure electron plasma in the hundreds of kHz range, no compression is observed. (Recall in [17] that the electron plasma was compressed with or without the presence of the antiprotons). This implies that in the present case, the antiproton compression was caused by the RW field directly coupling to the antiprotons, rather than being mediated by compression of the electron plasma. On the other hand, when no electrons are present and the RW is applied to a pure antiproton cloud, no compression is observed. Antiprotons are lost from the trap, perhaps indicating that they are heated by the RW field in the absence of a cooling medium.

The compression was studied as a function of RW frequency for antiproton-electron plasmas containing different numbers of electrons. Figure 5 shows the antiproton cloud central density, $n_{\overline{p}}$ (see Section 2.4), as a function of the RW frequency for different numbers of electrons.

One can see, for the 4×10^6 electrons case, that the antiproton cloud compresses for RW frequencies in the range 50–200 kHz. With increasing numbers of electrons, the maximum frequency at which compression is observed increases. Moreover, higher central densities are achieved with larger numbers of electrons. We note that the antiproton cloud does not compress well above ~ 700 kHz, which is similar to the lowest frequency at which the pure electron plasma compresses.

4 Bounce resonant transport of antiprotons

In many experiments, the RW field couples to Trivelpiece-Gould (TG) modes of the plasma, thereby applying a torque and leading to radial compression of the plasma [22, 23]. However, the lowest TG mode frequency of the electron plasma studied here is ~ 15 MHz, and therefore this mechanism is not consistent with the observed compression.

At first glance, compression by magnetron sideband cooling seems to provide an explanation for the data, because the sum of the magnetron (~ 1 kHz) and axial bounce (~ 270 kHz) frequencies of the antiprotons is close to the compression frequency [24–27]. Magnetron sideband cooling requires harmonic potentials, although compression has recently been achieved for independent particles in a slightly anharmonic potential [28]. This mechanism is unlikely to be responsible for the observed compression, because the space charge of the electrons greatly distorts the potential and it becomes highly anharmonic.

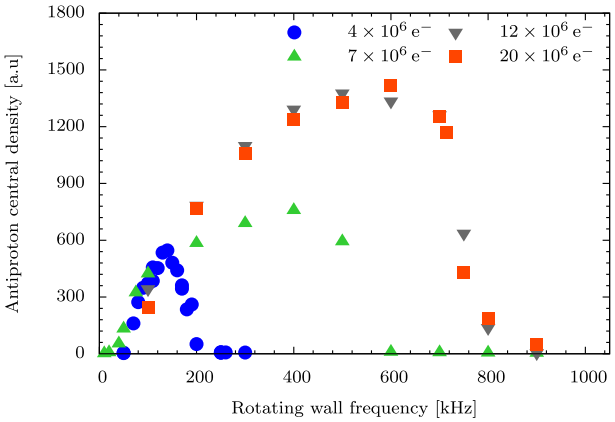

Fig. 5 Antiproton central density after applying the RW for 100 s, at 1 V and at a chosen frequency (with 0.2 kHz sweep). Different number of electrons are used, while the antiproton number remains the same at $\sim 1.5 \times 10^5$. The error bars are too small to be visible

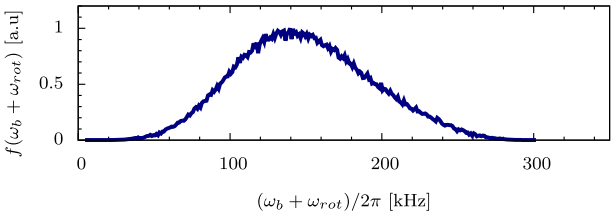

Fig. 6 The distribution of $(\omega_b + \omega_{rot})$ for antiprotons cooled by 4×10^6 electrons

For particles moving in an asymmetric time-varying potential (such as a RW), it has been observed that resonances between the particle's motional frequency and the drive frequency can result in radial inward or outward movement [29–33]. We have investigated whether this mechanism can be responsible for the compression described in Section 3. The antiproton bounce frequency, ω_b, was calculated by integrating the one-dimensional equations of motion in the self-consistent electric potential (see Fig. 2). Taking into account the distributions of radial positions and thermal energies allows a distribution of the antiproton bounce frequencies to be built up. The rotation frequency, ω_{rot}, of the antiproton-electron plasma was calculated from the self-consistent electric potential, and is dominated by the density of the electron plasma.

Figure 6 shows the combined distribution, $f(\omega_b + \omega_{rot})$, of the antiprotons when cooling with 4×10^6 electrons. This is the simplest system, since the electron plasma can be assumed to remain constant during the application of the RW. This assumption is supported by the fact that a compressed electron plasma is not visible in Fig. 4b. We observe that $f(\omega_b + \omega_{rot})$ lies over the same range of frequencies (50 – 200 kHz) as the observed compression. This indicates that bounce resonant transport may be a viable explanation for our data. When using a larger number of electrons, the system becomes more complex. The electron plasma compresses over time, with the result that both the rotation frequency and the shape of the potential well change dynamically. Compression of the electron plasma would increase ω_{rot} and consequently shift $f(\omega_b + \omega_{rot})$ to higher frequencies. This is qualitatively consistent with our observations, but further work is needed before a definitive conclusion can be made.

5 Conclusion

We have observed a new regime of compression of antiproton clouds, where the effect is not mediated by the compression of an electron plasma. We have investigated the compression as a function of the RW frequency and the number of electrons used to provide cooling. It is suggested that the compression may be explained by the bounce resonant transport of the antiprotons.

Acknowledgments This work was supported by: CNPq, FINEP/RENAFAE (Brazil); ISF (Israel); FNU (Denmark); VR (Sweden); NSERC, NRC/TRIUMF, AITF, FQRNT (Canada); DOE, NSF, LBNL-LDRD (USA); and EPSRC, the Royal Society and the Leverhulme Trust (UK). We are grateful for the efforts of the CERN AD team, without which these experiments could not have taken place. We acknowledge the valuable work of J. Strachan and P. Morrall, from STFC Daresbury Laboratory, in the design and construction of the antiproton capture trap. We are grateful to the members of the UCSD Non-neutral Plasma and Positron Research teams for the helpful discussions, in particular to Prof. T.M. O'Neil, Prof. D.H.E. Dubin, Prof. C.F. Driscoll, Prof. F. Anderegg, Prof. J. Danielson and Prof. C. Surko.

References

1. Holzscheiter, M.H., Charlton, M., Nieto, M.M.: Phys. Rep. **402**, 1–101 (2004)
2. Andresen, G.B., et al.: Phys. Lett. B **685**, 141 (2010)
3. Andresen, G.B., et al.: Nature **468**, 673 (2010)
4. Andresen, G.B., et al.: Nat. Phys. **7**, 558 (2011)
5. Amole, C., et al.: Nature **483**, 439 (2012)
6. Dubin, D.H.E., O'Neil, T.M.: Rev. Mod. Phys. **71**, 87 (1999)
7. Amoretti, M., et al.: Nature **419**, 456 (2002)
8. Malmberg, J.H., Driscoll, C.F.: Phys. Rev. Lett. **44**, 654 (1980)
9. Eggleston, D.L., O'Neil, T.M., Malmberg, J.H.: Phys. Rev. Lett. **53**, 982 (1984)
10. Notte, J., Fajans, J.: Phys. Plasmas **1**, 1123 (1994)
11. Huang, X.-P., et al.: Phys. Plasmas **5**, 1656 (1998)
12. Huang, X.-P., et al.: Phys. Rev. Lett. **78**, 875 (1997)
13. Jonsell, S., et al.: J. Phys. B: At. Mol. Opt. Phys. **42**, 215002 (2009)
14. Amole, C., et al.: Nucl. Instr. and Meth. A **735**, 319 (2014)
15. Gilson, E.P., Fajans, J.: Phys. Rev. Lett. **90**, 015001 (2003)
16. Fajans, J., et al.: Phys. Plasmas **15**, 032108 (2008)
17. Andresen, G.B., et al.: Phys. Rev. Lett. **100**, 203401 (2008)
18. Kuroda, N., et al.: Phys. Rev. Lett. **100**, 203402 (2008)
19. Andresen, G.B., et al.: Rev. Sci. Inst. **80**, 123701 (2009)
20. Gabrielse, G., et al.: Phys. Rev. Lett. **63**, 1360 (1989)
21. Andresen, G.B., et al.: Phys. Rev. Lett. **106**, 145001 (2011)
22. Trivelpiece, A.W., Gould, R.W.: J. App. Phys. **30**, 1784 (1959)
23. Anderegg, F., et al.: Phys. Rev. Lett. **81**, 4875 (1998)
24. Wineland, D., Dehmelt, H.: Int. J. Mass Spectrom. Ion Phys. **16**, 338 (1975)
25. Brown, L.S., Gabrielse, G.: Rev. Mod. Phys. **58**, 233 (1986)
26. Kellerbauer, A., et al.: Phys. Rev. A **73**, 062508 (2006)
27. Isaac, C.A., et al.: Phys. Rev. Lett. **107**, 033201 (2011)
28. Deller, A., et al.: New. J. Phys. **16**, 073028 (2014)
29. Eggleston, D.L., O'Neil, T.M.: Phys. Plasmas **6**, 2699 (1999)
30. Greaves, R.G., Surko, C.M.: Phys. Plasmas **8**, 1879 (2001)
31. Eggleston, D.L., Carrillo, B.: Phys. Plasmas **9**, 786 (2002)
32. Eggleston, D.L., Carrillo, B.: Phys. Plasmas **10**, 1308 (2003)
33. Greaves, R.G., Moxom, J.M.: Phys. Plasmas **15**, 072304 (2008)